HYL1-CLEAVAGE SUBTILASE 1 (HCS1) suppresses miRNA biogenesis in response to light-to-dark transition

Hyun Ju Jung[a,1], Suk Won Choi[a,1], Kyung-Hwan Boo[b,1], Jee-Eun Kim[a], Young Kyoung Oh[a], Min Kyun Han[a], Moon Young Ryu[c], Chang Woo Lee[c], Christian Møller[a], Pratik Shah[a], Gu Min Kim[a], Woorim Yang[a], Seok Keun Cho[c,2], and Seong Wook Yang[a,2]

[a]Department of Systems Biology, Institute of Life Science and Biotechnology, Yonsei University, Seoul 120-749, Korea; [b]Subtropical/Tropical Organism Gene Bank, Department of Biotechnology, College of Applied Life Science, Jeju National University, Jeju 63243, Korea; and [c]Xenohelix Research Institute, Incheon 21984, Korea

Edited by Xuemei Chen, Botany and Plant Sciences, University of California, Riverside, CA; received September 19, 2021; accepted December 16, 2021

The core plant microprocessor consists of DICER-LIKE 1 (DCL1), SERRATE (SE), and HYPONASTIC LEAVES 1 (HYL1) and plays a pivotal role in microRNA (miRNA) biogenesis. However, the proteolytic regulation of each component remains elusive. Here, we show that HYL1-CLEAVAGE SUBTILASE 1 (HCS1) is a cytoplasmic protease for HYL1-destabilization. HCS1-excessiveness reduces HYL1 that disrupts miRNA biogenesis, while HCS1-deficiency accumulates HYL1. Consistently, we identified the HYL1^{K154A} mutant that is insensitive to the proteolytic activity of HCS1, confirming the importance of HCS1 in HYL1 proteostasis. Moreover, HCS1-activity is regulated by light/dark transition. Under light, cytoplasmic CONSTITUTIVE PHOTOMORPHOGENIC 1 (COP1) E3 ligase suppresses HCS1-activity. COP1 sterically inhibits HCS1 by obstructing HYL1 access into the catalytic sites of HCS1. In contrast, darkness unshackles HCS1-activity for HYL1-destabilization due to nuclear COP1 relocation. Overall, the COP1-HYL1-HCS1 network may integrate two essential cellular pathways: the miRNA-biogenetic pathway and light signaling pathway.

subtilisin-like protease | miRNA biogenesis | COP1 E3 ligase | HYL1 proteostasis | light/dark transition

MicroRNAs (miRNAs) are a class of small noncoding regulatory RNAs that play key roles in mRNA degradation and translational suppression in eukaryotes (1–5). In animals, the core microprocessor complex minimally consists of Drosha and DiGeorge SYNDROME CHROMOSOMAL REGION 8 (DGCR8), which cleaves primary miRNAs (pri-miRNAs) to precursor miRNAs (pre-miRNAs) in the nucleus (6–8). Pre-miRNAs are then exported to the cytoplasm and further processed into mature miRNAs through Dicer and TRANSACTIVATION RESPONSE ELEMENT RNA-BINDING PROTEIN (TRBP) (9). In plants, miRNAs are processed by the core microprocessor, including DICER-LIKE 1 (DCL1), SERRATE (SE), and HYPONASTIC LEAVES 1 (HYL1), from highly variable stem regions of pri-miRNAs (10–13). The processed miRNAs are loaded onto ARGONAUTE (AGO) proteins, the kernel of diverse RNA-INDUCED GENE SILENCING COMPLEXES (RISCs), to cleave or translationally supress target mRNAs, that has been commonly coopted by plants and animals (14–16). Many studies have further focused on defining interactive proteins, by which the microprocessor components and RISCs can be intricately modulated for miRNA biogenesis and miRNA-induced gene silencing (17–19).

Proteolysis is an essential regulatory layer for the proteomic adjustment of eukaryotic development, growth, and accommodation to ever-changing environmental conditions (20, 21). Many studies have suggested that autophagy and the ubiquitin-26S proteasome system (UPS) participate in the proteolytic regulation of microprocessor components and RISCs. In animals, AGO1, Dicer, and AGO2 were reported to be degraded by autophagy (22). Drosha and TRBP are regulated by the UPS (23, 24). On the other hand, recent studies have shown that AGO2 is also degraded by the UPS upon poly-ubiquitination by cullin-RING E3 ubiquitin ligase (25, 26). In plants, F-BOX WITH WD40 2 (FBW2) targets AGO1 for autophagy-mediated degradation (27). The F-box protein P0 of polerovirus mediates AGO1, AGO2, AGO4, and AGO9 for degradation through autophagy (28–31). The AGO1 DUF domain is required for P0-mediated degradation (32). P0 also triggers endoplasmic reticulum (ER)-derived autophagy for the removal of membrane-bound AGO1 (33). Moreover, the RNA-binding protein P25 of potato virus X mediates AGO1 degradation through the proteasome (34). CURLY LEAF (CLF) negatively regulates FBW2, which in turn triggers AGO1 degradation in conditions of CLF deficiency, but this degradation is blocked by the proteasome inhibitor (35). Although autophagy and the proteasome appear to be involved in the proteolytic regulation of RISCs in plants, the compatibility between the two conventional pathways, either in the viral or nonviral context, is still ambiguous and requires further investigation.

Previously, we reported that HYL1 is degraded by an unidentified protease (36). We further showed that HYL1 is a nuclear-cytoplasmic shuttling protein in response to light/dark transition and phosphorylated HYL1 could be proportionally retained in the nucleus, which protects HYL1 degradation in

Significance

HYPONASTIC LEAVES 1 (HYL1)-CLEAVAGE SUBTILASE 1 (HCS1) is a novel negative regulator of microRNA (miRNA) biogenesis that degrades HYL1 in the cytoplasm. Furthermore, cytoplasm CONSTITUTIVE PHOTOMORPHOGENIC 1 (COP1) E3 ligase inhibit HCS1-mediated HYL1 degradation. The COP1-HYL1-HCS1 network may integrate two essential cellular pathways: the miRNA-biogenetic pathway and light signaling pathway. Our finding suggests a regulatory pathway in the miRNA-biogenetic system.

Author contributions: S.K.C. and S.W.Y. designed research; H.J.J., S.W.C., K.-H.B., J.-E.K., Y.K.O., M.K.H., M.Y.R., P.S., G.M.K., and W.Y. performed research; H.J.J., S.W.C., K.-H.B., C.W.L., and C.M. analyzed data; and H.J.J., S.K.C., and S.W.Y. wrote the paper.

The authors declare no competing interest.

This article is a PNAS Direct Submission.

[1]H.J.J., S.W.C., and K.-H.B. contributed equally to this work.

[2]To whom correspondence may be addressed. Email: chosk@xenohelix.com or yangsw@yonsei.ac.kr.

This article contains supporting information online at http://www.pnas.org/lookup/suppl/doi:10.1073/pnas.2116757119/-/DCSupplemental.

Published February 4, 2022.

darkness (37). Moreover, we suggested that DCL1 can be degraded by an unknown protease during skotomorphogenesis and light/dark conversion (38). Furthermore, damaged SE is degraded by ubiquitin-independent proteasomal activity (39). Intriguingly, a recent study suggested that Dicer is cleaved by an unknown serine protease in undifferentiated monocytes (40, 41). These studies indicated that unidentified proteases and unknown mechanisms, beyond autophagy and the UPS, exist for microprocessor turnover in plants and animals. To understand the proteolytic regulation of the microprocessor components, we primarily focused on identifying the mechanism by which HYL1 is degraded. Among the over 800 proteases encoded in the *Arabidopsis* genome, we systemically located the protease that specifically degrades HYL1. Here, we show that HYL1-CLEVAGE SUBTILASE 1 (HCS1) is a cytoplasmic subtilisin-like protease. In darkness, HCS1 vigorously eliminates HYL1. In contrast, under light, COP1 E3 ligase inhibits HCS1, irrespective of its role in the UPS; thus, HYL1 accumulates. Collectively, we identify not only a protease of HYL1 destabilization, but also reveal an integrative regulatory network among miRNA biogenesis and the light signaling pathway.

Results

HCS1 Is a Primary Protease for HYL1 Degradation. To identify the unknown protease for HYL1-degradation, we performed a cell-free HYL1 degradation assay using the crude extract from 10-d-old WT seedlings and recombinant HYL1 proteins with two different epitope-tags: a 2B8-tag at the N-terminal and a six-histidine (6His) tag at the C-terminal end (Fig. 1*A*). Then, the cleaved HYL1 fragment was purified and analyzed by liquid chromatography/tandem mass spectrometry (LC-MS/MS). In the LC-MS/MS analysis, we found that trypsin-digested HYL1 fragments end at the position of the fourth fragment (VTQ FTCTVEICGIK) and the fifth trypsin-digested fragment (TALLAIQSDTK). The estimated molecular weight of the two fragments (amino acids 1 to 144 and 1 to 173) with 2B8 epitope and linkers were around 23 to 25 kDa, used for LC-MS/MS analysis (Fig. 1*B* and *SI Appendix*, Fig. S1*A*). The two analyzed fragments approximately coincided with the molecular weight of the observed N-terminal cleaved fragments in the cell-free degradation assay. These results indicated that the cleavage sites could exist between 144 and 173 amino acids of HYL1. Using ProP1.0 and ExPASy peptidecutter programs, we found three putative target sites for subtilases in the region between the fourth and fifth fragments (Lys153, Lys154, and Lys173 amino acids). This analysis implied that the unknown protease for HYL1 degradation could be a member of the subtilase family (*SI Appendix*, Fig. S1*B*).

There are 56 subtilases in *Arabidopsis*, which are classified into six clades (*SI Appendix*, Fig. S1*C*). To clarify which of these subtilases are involved in modulating the half-life of HYL1, we further investigated the transcriptome of 10-d-old WT/*35S:HYL1-6Myc* transgenic plants as compared to WT plants, with the reasoning that a HYL1-specific protease could be modulated in response to excessive or deficient HYL1 (Fig. 1*C*). Comparison of 27,372 genes between WT/*35S:HYL1-6Myc* and WT revealed that 155 genes were differentially expressed by at least a twofold change ratio ($\log_2\Delta$FPKM, fragments per kilobase per million mapped reads) (*SI Appendix*, Fig. S1*D*). Among the 285 annotated proteases in the transcriptome data, we found that only five proteases were up-regulated in WT/*35S:HYL1-6Myc* transgenic plants by over twofold, and four of them were subtilases: *SBT4.4*, *SBT3.3*, *SBT3.7*, and *SBT5.4* (Fig. 1*D*). In addition to these four subtilases, we identified 14 candidates by excluding 38 of the 56 subtilases, as these were hardly expressed or decreased in WT or WT/*35S:HYL1-6Myc* transgenic plants, respectively (Fig. 1*D*). To determine the correlation between the expression of the selected 18 genes and *HYL1* transcript levels, we further conducted droplet digital PCR (dd-PCR) analysis using WT, WT/*35S:HYL1-6Myc*, and *hyl1-2* mutant seedlings. Again, we found that the four aforementioned subtilases were distinctively up-regulated in WT/*35S:HYL1-6Myc* but down-regulated in *hyl1-2* (Fig. 1*E* and *SI Appendix*, Fig. S1*E*).

Next, we transiently expressed the 4 subtilase genes as the major candidates and 20 subtilase genes as controls in tobacco leaves (*SI Appendix*, Fig. S2*A*). Then, we performed a cell-free HYL1 degradation assay using tobacco crude extracts harboring each expressed subtilase with a 6Myc epitope. Of the 24 subtilases, we found that SBT5.4 most efficiently degrades HYL1, while SBT5.3 shows relatively weak cleavage activity compared to SBT5.4 (*SI Appendix*, Fig. S2*B*). To ensure the specificity of the subtilases, we conducted an in vitro HYL1 cleavage assay by incubating recombinant HYL1 and the immunoprecipitated SBT5.4 and SBT5.3 using α-Myc antibody, expressed in tobacco leaves. We observed that SBT5.4 and SBT5.3 produced the N-terminal fragment of HYL1, as seen in the cell-free degradation assay (Fig. 1*A*), confirming their specificity for HYL1 degradation (Fig. 1 *F* and *G* and *SI Appendix*, Fig. S2*C*). Previously, two studies reported the physiological features of SBT5.3 and SBT5.4 (Fig. 1*H*). The former, known as *AIR3*, is functionally downstream of *NAC1* for root development (42), and the latter drives the CLAVATA phenotype when overexpressed (43). However, the target proteins and detailed functionality of these proteases remained unclear. Hence, we designated SBT5.4 as HCS1, which showed HYL1 degradation activity.

Next, to recapitulate the enzyme specificity of HCS1 and AIR3 in *Arabidopsis*, we generated overexpressed HCS1 and AIR3, and immunopurified proteases using α-Myc antibody. By applying recombinant 2B8-HYL1-6His (0.2 μg) as a substrate, we performed an in vitro HYL1 cleavage assay by increasing the concentration of the purified HCS1-6Myc and AIR3-6Myc (0.15 to 1.5 μg) (Fig. 1 *I* and *J* and *SI Appendix*, Fig. S2*D*). As seen in the tobacco assay system, HCS1-6Myc showed much higher proteolytic activity than AIR3-6Myc in *Arabidopsis* (Fig. 1*K*). To confirm the N-terminal cleavage, we performed an in vitro HYL1 cleavage assay with recombinant 6His-HYL1 (0.2 μg) as a substrate by either extending incubation time (*SI Appendix*, Fig. S2*E*) or by increasing the concentration of the purified HCS1-6Myc (*SI Appendix*, Fig. S2*G*).

To further characterize the enzyme kinetics of HCS1, we used an internally quenched fluorescent (IQF) peptide substrate with a fluorophore (FAM) and a quencher (DABCYL) at opposite ends of the mimic peptide (Fig. 1*L*). We optimized the monitoring wavelength of fluorescence (520 nm) and the concentration of HCS1 (1 μM) for the assay. Then, by increasing the incubation time or substrate concentration, we determined that the K_m value of substrate was 0.9512 μM and K_{cat} value was 0.68 μM (Fig. 1 *M* and *N* and *SI Appendix*, Fig. S2 *I* and *J*). As shown in Fig. 1*B*, HYL1 has three potential cleavage sites for subtilases at amino acids Lys153, Lys154, and Lys173. Among them, the Lys154 residue has the highest probability for subtilase cleavage (ProP1.0 program). To confirm the cleavage sites, we substituted the lysine residues of predicted sites with alanine residues to generate 2B8-HYL1^{K153A}-6His, 2B8-HYL1^{K154A}-6His, 2B8-HYL1^{K173A}-6His, and combinatorial double and triple HYL1 mutants. Then, we performed an in vitro degradation assay by incubating immune-purified (IP) HCS1-6Myc (1 μM) with the recombinant HYL1 mutants. Consistent with the prediction of the program, the 2B8-HYL1^{K154A}-6His mutant showed the strongest resistance, while the 2B8-HYL1^{K153A}-6His mutant displayed the second strongest resistance to the proteolytic activity of HCS1. The degradation of HYL1 by HCS1-6Myc was not hindered by the

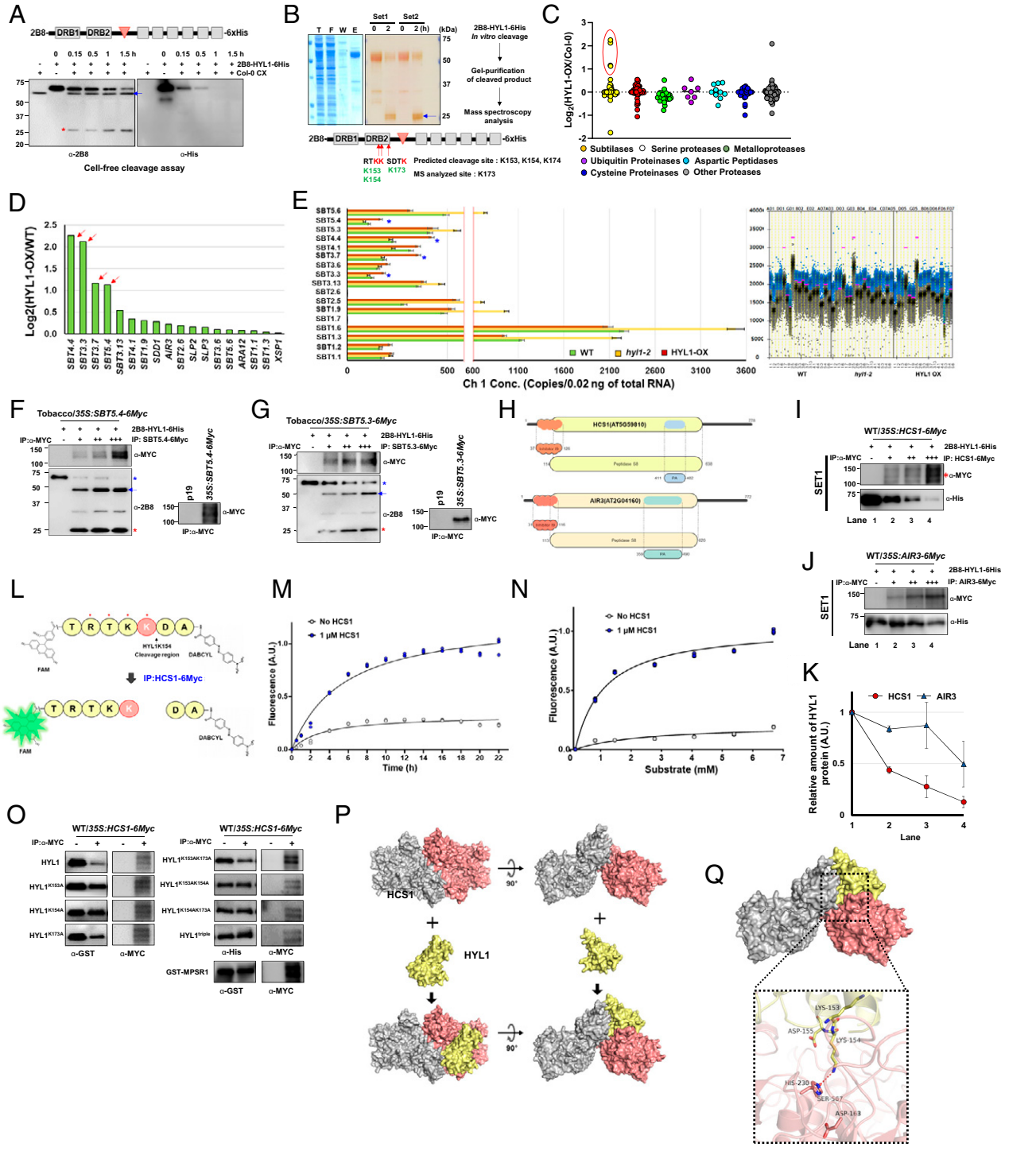

Fig. 1. HYL1 protein is cleaved by HCS1 protease. (*A*) Cell-free cleavage assay using recombinant 2B8-HYL1-6His protein and WT crude extract. Blue arrow indicates 2B8-specific protein in the crude extract, which is used as a loading control. Red asterisk indicates the cleaved N-terminal fragment of HYL1. (*B*) Identification of HYL1 cleavage site by LC-MS/MS analysis. Blue arrow indicates the cleaved N-terminal fragment of HYL1. (*C*) Expression profiling of proteases in *35S:HYL1-6Myc* plants by transcriptome analysis. (*D*) Expression profiling of up-regulated SBTs in *35S:HYL1-6Myc* plants by transcriptome analysis. Red arrow indicates the high increased proteases. (*E*) ddPCR analyses show the expression levels of subtilisin-like proteases (SBTs) in *hyl1-2* and *35S:HYL1-6Myc* plants. Blue asterisk indicates the four candidate SBTs. The data shown are the averages of three replicates ± SD ($n = 3$). (*F* and *G*) In vitro cleavage assay using IP-HCS1-6Myc and IP-AIR3-6Myc from tobacco leaves. The blue asterisk indicates noncleaved HYL1 and the red asterisk indicates the N-terminal cleaved HYL1 form. The blue arrow indicates the heavy chain of the α-Myc antibody. (*H*) Schematic protein domains of HCS1 and AIR3. (*I* and *J*) In vitro cleavage assay of the full-length HYL1 using IP-HCS1-6Myc and IP-AIR3-6Myc. The red asterisk indicates the active form of HCS1-6Myc. (*K*) The relative HYL1 levels in the average value of three biological replicates were calculated by ImageJ software. Error bars indicate ± SD ($n = 3$). (*L*) Schematic of HYL1 peptide substrate including fluorophore (FAM) and quencher (DABCYL). (*M* and *N*) In vitro cleavage assay of the IQF peptide substrate using IP-HCS1-6Myc. (*O*) In vitro cleavage assay of HYL1 and HYL1 mutant proteins using IP-HCS1-6Myc. (*P*) Surface representation of HCS1 dimer and HYL1 complex. Monomeric HCS1 and HYL1 are colored as salmon and pale yellow, respectively. (*Q*) Expansion predicted the structure of HYL1K154 cleaved region in the active site of HCS1. Interacting residues of HYL1 and the catalytic triad of HCS1 are presented as a stick model.

substitution of Lys173 amino acid (Fig. 1*O*). We confirmed the importance of Lys154 by performing in vitro HYL1 cleavage assay using recombinant 6His-HYL1^{K154A} as a substrate (*SI Appendix*, Fig. S2 *F* and *H*).

Several studies have characterized the structure of SISBT3 and cucumisin by X-ray crystallography; these studies have reported that the protease-associated (PA) domain has a function in the homodimerization of subtilase, which is a prerequisite for enzyme activation (44–52). Rose et al. (53) further reported that the crystal structure of SISBT3 (PDB ID code 3I6S) can serve as a paradigm for most of the subtilases in *Arabidopsis*. Thus, to define the structural features of HCS1 and its target recognition, we first tested whether HCS1 forms a homodimer for its activity using size-exclusion chromatography. We observed that MBP-HCS1-3HA predominantly forms a homodimer (*SI Appendix*, Fig. S3*A*). Second, we adopted the SISBT3 structure as a template to produce the homology model of HCS1 using SWISS-MODEL. The predicted model of HCS1 has a root mean square deviation value of 0.242 with SISBT3 (*SI Appendix*, Fig. S3*B*). Third, we adopted the crystal structures of double-stranded RNA-binding domains of HYL1 (54) (*SI Appendix*, Fig. S3*C*). Using the structural information of HYL1 and HCS1, we performed structural modeling of how HYL1 is recognized by the HCS1 dimer. The binding models were constructed using the program HEX (55) and the high ambiguity-driven protein–protein DOCKing (HADDOCK) online server (56) (Fig. 1*P* and *SI Appendix*, Fig. S3*D*). The selected best docking model showed that dsRBD2 of HYL1 fitted in the active site (Asp163, His230, and Ser567) of HCS1. In detail, the helix region of dsRBD2 headed toward the active site and was located in the substrate-binding pocket of HCS1 (Fig. 1*Q*). Consistently, the peptide bond between Lys154 and Asp155, which has the highest probability for HCS1 cleavage, was located in the helix region of dsRBD2, which tends to face the negatively charged active site of HCS1. The 3.5 Å distance between Lys154 of HYL1 and Ser567 of HCS1 is suitable for recognition and cleavage. The structural modeling and biochemical assays indicate that HCS1 cleaves Lys154 in the DRB2 domain of HYL1.

HCS1 Is a Negative Regulator of miRNA Biogenesis. For loss-of-function analyses of *HCS1* and *AIR3*, we isolated two T-DNA insertion mutants for *hcs1*, *hcs1-1* (salk_150825) and *hcs1-2* (salk_025087), and one T-DNA mutant for *air3* (salk_125788), and then crossed *hcs1-1* and *air3* to generate *hcs1air3* double mutants (*SI Appendix*, Fig. S4 *A* and *B*). We observed that the HYL1 level was notably increased in the *hcs1-1* and *hcs1-2* single mutants (>1.5-fold), but only slightly increased in *air3* (Fig. 2*A* and *SI Appendix*, Fig. S4*D*). However, *hcs1air3* remarkably accumulated HYL1 as compared to WT (>3.9-fold), which was possibly caused by the functional redundancy and competency of AIR3 in the absence of HCS1 (Fig. 2*B*). We also found that *AIR3* transcripts were dramatically up-regulated by *HCS1* deficiency, showing an epistatic relationship between two paralogous genes (*SI Appendix*, Fig. S4*C*). We also tested that the accumulated HYL1 in the *hcs1* drops to a normal state by expressing the *35S:AIR3-6Myc* transgene (*SI Appendix*, Fig. S4*E*).

Next, we conducted the cycloheximide-chase assay to monitor the half-life of HYL1 in *hcs1air3*. HYL1 was rapidly destabilized in WT but fully retained in *hcs1air3*, confirming that HCS1 is a bona fide protease of HYL1, and AIR3 could be an auxiliary protease (Fig. 2 *C* and *D*). To verify the cellular localization of the proteases, we constructed WT/*35S:HCS1-YFP* and WT/*35S:AIR3-YFP* transgenic plants and observed that HCS1-YFP and AIR3-YFP localize in the cytoplasm (Fig. 2*E*). Each single mutant, *hcs1* and *air3*, showed minor defects in phyllotaxy, while *hcs1air3* showed more defects in both phyllotaxy and leaf development (Fig. 2*F* and *SI Appendix*, Fig. S4 *F*–*M*). Similar defective phenotypes were observed in WT/*35S:HYL1-6Myc* transgenic plants, when they highly accumulate heterologous HYL1-6Myc and endogenous HYL1 (*SI Appendix*, Fig. S4 *M* and *N*). Consistently, small RNA blot analysis showed that several miRNAs were reduced in the *hcs1air3* (Fig. 2*G* and *SI Appendix*, Fig. S5*A*).

To recapitulate the defected miRNA levels in *hcs1air3*, we performed small RNA-sequencing analysis with *hcs1air3*, *hyl1-2*, and WT seedlings. The median expression level of miRNAs in the *hcs1air3* and *hyl1-2* mutants, shown as the change ratio ($\log_2\Delta$readcounts per 10 million [RPTM]), was −0.48 and −1.98, respectively (Fig. 2*H*). Of the 173 miRNAs with a total expression of at least 10 RPTM, over 84% and 81% of the miRNAs displayed lower expression in the *hcs1air3* and *hyl1-2* seedlings, respectively, when compared to that of WT seedlings. (*SI Appendix*, Fig. S5*B*). Next, we compared differentially expressed miRNAs between the *hcs1air3* and *hyl1-2* mutants. The *hcs1air3* and *hyl1-2* mutants shared 5 up-regulated miRNAs and 124 down-regulated miRNAs (Fig. 2*I*). However, the degree of miRNA drops in the *hcs1air3* was minor compared to that of *hyl1-2*. Based on these results, we assumed that the dysregulation of HYL1 proteostasis might slightly affect miRNA biogenesis and plant development.

For gain-of-function analyses, we monitored the WT/*35S:HCS1-6Myc* and WT/*35S:AIR3-6Myc* transgenic plants. The 10-d-old WT/*35S:HCS1-6Myc* seedlings showed severe developmental defects compared to the relatively normal development of WT/*35S:AIR3-6Myc* seedlings (Fig. 2 *J* and *K*). The phenotypes of the transgenic plants were correlated to HYL1 levels. We found that excessive HCS1 dramatically reduced HYL1 and excessive AIR3 slightly diminished HYL1, showing the auxiliary function of AIR3 (Fig. 2 *L* and *M*). In accordance with the defective phenotypes, excessive HCS led to reduced accumulation of developmentally essential miRNAs (Fig. 2*N* and *SI Appendix*, Fig. S5*C*). To confirm the miRNA reductions, we further performed miRNAtome analysis using the Illumina sequencing platform. The expression of miRNAs in the two lines with excess HCS1, #12 and #57, was dramatically reduced compared with that in the WT (median change-ratio: $\log_2\Delta$RPTM value of −3.95 for #12 and −4.93 for #57) (Fig. 2*O*). Of the 146 miRNAs that had a total expression of at least 50 RPTM, nearly 99% of the miRNAs had lower expression in both seedlings #12 and #57 (Fig. 2*P*). The expression of miRNAs reduced in WT/*35S:HCS1-6Myc* #12 and *hyl1-2* seedlings by the second sequencing (median change-ratio: $\log_2\Delta$RPTM value of −1.23 for #12 and −3.29 for *hyl1-2*) (*SI Appendix*, Fig. S5*D*). Taken together, these results suggest that HCS1 is a novel negative regulator of HYL1.

Light Deprivation Unshackles HCS1 to Degrade HYL1. HYL1 and DCL1 are rapidly degraded by light-deprived conditions, such as shade, darkness, and during the prolonged etiolation process (36–38). Since light signaling integrates into miRNA biogenesis through the proteolytic regulation of core microprocessor components, we investigated whether HCS1 is responsible for the HYL1-degradation in light-deprived conditions. WT, *hcs1*, *air3*, and *hcs1air3* seedlings were grown for 10 d under continuous light (80 μmol m^{-2} s^{-1}) and then transferred to dark conditions for 12 h, after which the nuclear relocation of COP1 could be sufficiently stimulated. After 12 h of light deprivation, HYL1 dramatically decreased in WT, *hcs1*, and *air3*, while HYL1 was fully maintained in *hcs1air3* (Fig. 3 *A* and *B*). In the light/dark transition, *HYL1* transcripts were unchanged in WT, *hcs1,* and *air3*. *HYL1* transcripts were reduced in *hcs1air3* under both light and dark conditions, showing a possible feedback regulation (*SI Appendix*, Fig. S6*A*). In addition, *HCS1* and *AIR3* transcripts were accumulated as a result of the light/dark transition (*SI Appendix*, Fig. S6*B*).

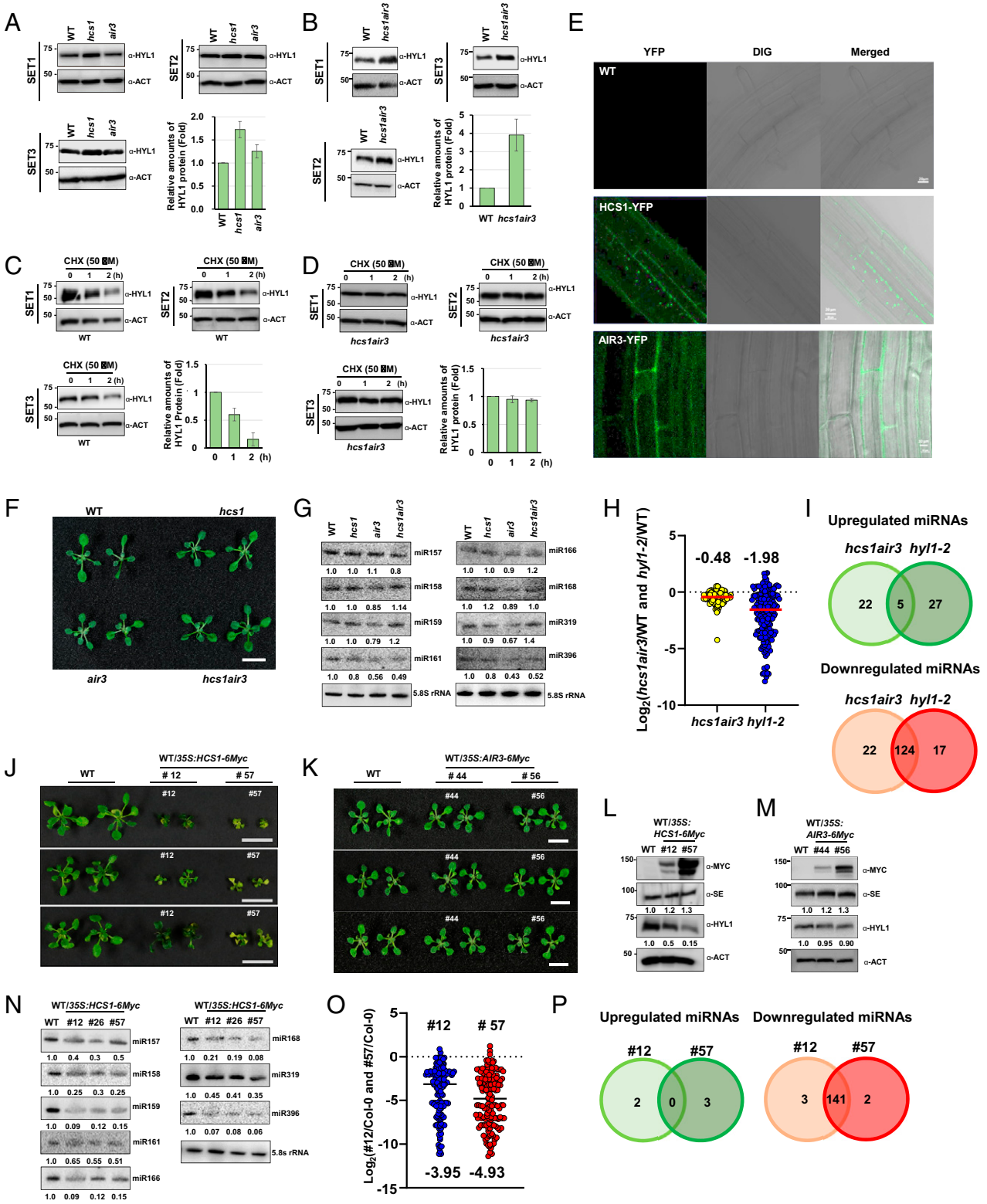

Fig. 2. HCS1 dysregulation affects miRNA biogenesis and plant development. (*A*) The levels of HYL1 in *hcs1* and *air3*. (*B*) The level of HYL1 in *hcs1air3*. (*C*) In vivo protein decay assay using cycloheximide (CHX) in WT. (*D*) In vivo protein decay assay using CHX in *hcs1air3*. Actin was used as a loading control. Data are the averages of independent biological replicates ± SD ($n = 4$). (*E*) Cellular localization of HCS1-YFP and AIR3-YFP in 5-d-old transgenic plants. (*F*) Phenotype analysis of *hcs1*, *air3*, and *hcs1air3*. (*G*) Small RNA blot analysis of *hcs1*, *air3*, and *hcs1air3*. (*H* and *I*) miRNAtome analysis. Median expression levels of miRNAs in *hcs1air3* and *hyl1-2* as compared to WT seedlings. Change ratio ($\log_2\Delta$TPTM) is displayed in the *y* axis (*H*) and up- and down-regulated miRNA in *hcs1air3* and *hyl1-2* (*I*). (*J* and *K*) Phenotypes of *35S:HCS1-6Myc* and *35S:AIR3-6Myc* plants. Bars, 1 cm. (*L* and *M*) HCS1, SE, HYL1 levels in *35S:HCS1-6Myc* and *35S:AIR3-6Myc*. (*N*) Small RNA blot analysis of *35S:HCS1-6Myc* plants. (*O* and *P*) miRNAtome analysis. Median expression levels of miRNAs in *35S:HCS1-6Myc* lines (#12 and #57) as compared to WT seedlings (*O*) and up- and down-regulated miRNA in *35S:HCS1-6Myc* lines (*P*).

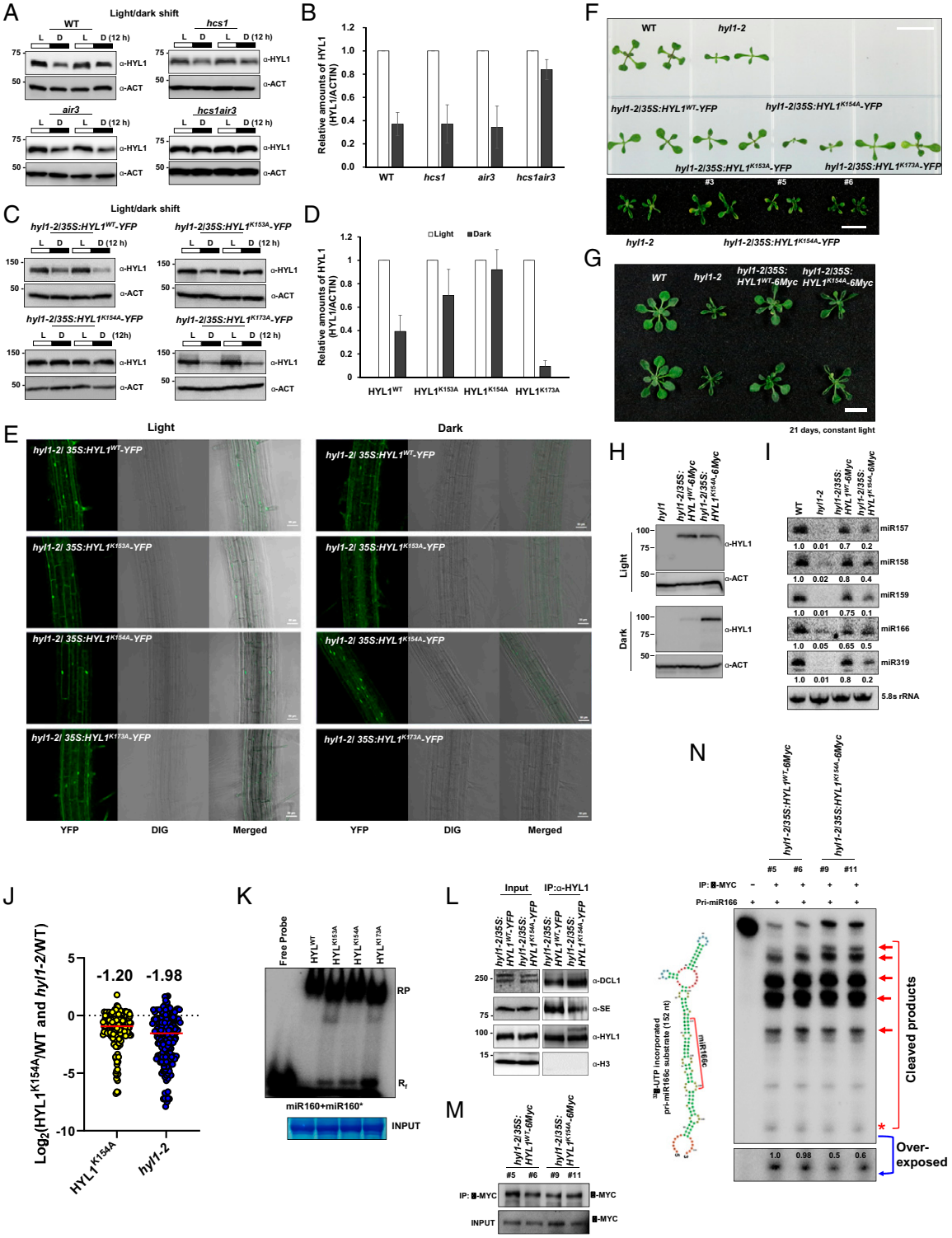

Fig. 3. HYL1^{K154A} is an essential residue for HYL1 proteostasis. (*A* and *B*) The levels of HYL1 in WT and *hcs1*, *air3*, and *hcs1air3* during the light/dark transition. (*C* and *D*) The levels of HYL1-YFP, HYL1^{K153A}-YFP, HYL1^{K154A}-YFP, and HYL1^{K173A}-YFP in the transgenic lines during the light/dark transition. Data are the averages of three biological replicates ± SD (n = 3). (*E*) Visualization of *HYL1-YFP*, *HYL1^{K153A}-YFP*, *HYL1^{K154A}-YFP*, or *HYL1^{K173A}-YFP* during the light/dark transition. YFP signals were monitored in 5-d-old seedling roots. (*F*) Phenotype analysis of WT, *hyl1-2*, *hyl1-2/35S:HYL1-YFP*, *HYL1^{K153A}-YFP*, *HYL1^{K154A}-YFP*, or *HYL1^{K173A}-YFP* in 10-d-old plants. (*G*) Phenotype analysis of *hyl1-2/35S:HYL1^{WT}-6Myc* and *HYL^{K154A}-6Myc* in 2-wk-old plants. Bars, 1 cm. (*H*) Expression levels of HYL1-6Myc and HYL1^{K154A}-6Myc during the light/dark transition. (*I*) Small RNA blot analysis of miRNAs in *hyl1-2/35S:HYL1-6Myc* and *HYL^{K154A}-6Myc* plants. (*J*) miRNAtome analysis. Median expression levels of miRNAs in *hyl1-2* and *HYL1^{K154A}-6Myc* as compared to WT seedlings. (*K*) EMSA of HYL1 and the other mutant proteins with ^{P32}α-UTP-labeled miR160/miRNA160*. (*L*) Co-IP of SE and DCL1 using HYL1-6Myc and HYL1^{K154A}-6Myc. Histon3 (H3) was used as a negative control. (*M*) The level of IP-HYL1-6Myc and IP-HYL1^{K154A}-6Myc. (*N*) Schematic structure of ^{P32}α-UTP-labeled pri-mR166c substrate and in vitro pri-miRNA processing assay. IP proteins were incubated with ^{P32}α-UTP-labeled pri-mR166c substrate for 3 h. Red arrows indicate the processed intermediates from pri-miR166c. The red asterisk marks miRNA166.

To further validate the role of HCS1 in dark-induced HYL1 degradation, we constructed transgenic plants expressing HYL1-YFP, HYL1^{K153A}-YFP, HYL1^{K154A}-YFP, or HYL1^{K173A}-YFP in the *hyl1-2* background. Then, we performed a light/dark transition assay using 10-d-old seedlings of the following transgenic plants: *hyl1-2/35S:HYL1-YFP*, *hyl1-2/35S:HYL1^{K153A}-YFP*, *hyl1-2/35S:HYL1^{K154A}-YFP*, and *hyl1-2/35S:HYL1^{K173A}-YFP*. HYL1-YFP was reduced by ∼60%, HYL1^{K153A}-YFP was reduced by ∼25%, and HYL1^{K173A}-YFP was decreased by almost 95% in the dark; HYL1^{K154A}-YFP showed no reduction (Fig. 3 *C* and *D*). Next, the dark-stable HYL1^{K154A}-YFP and HYL1^{K153A}-YFP were further visualized as compared to the dark-labile HYL1-YFP and HYL1^{K173A}-YFP. The fluorescence of HYL1^{K154A}-YFP was significantly accumulated in the nuclei even after 12 h in darkness, unlike the faded emissions from the WT and the other two mutants (Fig. 3*E* and *SI Appendix*, Fig. S6*C*). These results confirmed that HCS1 is responsible for dark-induced HYL1 degradation. Furthermore, we found that the Lys154 of HYL1 is a critical region for HCS1 mediated HYL1 degradation.

HYL1 Proteostasis Is Important for miRNA Biogenesis. While studying the transgenic plants, we found that *hyl1-2/35S:HYL1^{K154A}-YFP* displayed severe defects in seedling development as compared to those of *hyl1-2/35S:HYL1-YFP*, *hyl1-2/35S:HYL1^{K153A}-YFP*, and *hyl1-2/35S:HYL1 ^{K173A}-YFP* (Fig. 3*F* and *SI Appendix*, Fig. S6 *D* and *E*). To rule out the intervention of C-terminal YFP tagging in the HYL1 functionality, we reconstructed *hyl1-2/35S:HYL1-6Myc* and *hyl1-2/35S:HYL1^{K154A}-6Myc* transgenic plants. We found that the phenotypes of *hyl1-2/35S:HYL1^{K154A}-6Myc* are reminiscent of that of *hyl1-2*, such as hyponastic leaves, small siliques, and disruption in phyllotaxy (Fig. 3*G* and *SI Appendix*, Fig. S6 *F–J*). These findings confirm that the expression of invincible HYL1 hinders miRNA biogenesis. The developmental defects were correlated with the invincibility of HYL1^{K154A}-6Myc in darkness (Fig. 3*H*). Next, we found that the defective phenotypes of *hyl1-2/35S:HYL1^{K154A}-6Myc* were correlated with reduced levels of miRNAs (Fig. 3*I*). To test the defected miRNA levels in the *hyl1-2/35S:HYL1^{K154A}-6Myc*, we performed small RNA-sequencing analysis using the Illumina platform. The median expression level of miRNAs in the *hyl1-2/35S:HYL1^{K154A}-6Myc* and *hyl1-2*, expressed as the change ratio ($\log_2$ΔRPTM), was −1.20 and −1.98, respectively (Fig. 3*J*). Of the 173 miRNAs with a total expression of at least 10 RPTM, over 82% and 81% of the miRNAs displayed lower expression in the *hyl1-2/35S:HYL1^{K154A}-6Myc* and *hyl1-2* seedlings, respectively, compared to that of WT.

Next, we compared differentially expressed miRNAs between the *hyl1-2/35S:HYL1^{K154A}-6Myc* and *hyl1-2*. The *hyl1-2/35S:HYL1^{K154A}-6Myc* and *hyl1-2* mutants shared 13 up-regulated miRNAs and 124 down-regulated miRNAs (*SI Appendix*, Fig. S6 *K* and *L*). However, the median value drop in *hyl1-2* (−1.98) was slightly restored to 0.77 by expressing *35S:HYL1^{K154A}-6Myc*, showing the partial functionality of HYL1^{K154A} (Fig. 3*J*). To determine how HYL1^{K154A} impeded development and miRNA biogenesis, we performed a gel electromobility assay to determine the binding affinity of HYL1^{K154A} for miRNA/miRNA*. We found that HYL1^{K154A}, HYL1^{K153A}, and HYL1^{K173A} recognize radioisotope-labeled miR160/miR160* substrate (Fig. 3*K*). However, the binding affinity of HYL1^{K154A} ($5.0 \pm 1.34\ 10^{-8}$M) was slightly weaker than that of WT ($5.8 \pm 1.82\ 10^{-8}$M) (*SI Appendix*, Fig. S7 *A–D*). Furthermore, the coimmunoprecipitation (co-IP) assay showed that HYL1^{K154A} could form a microprocessor complex with SE and DCL1 in vivo (Fig. 3*L*). By performing in vitro pull-down assays, we confirmed that the interaction between SE or DCL1 and HYL1 ^{K154A} was similar to their respective interactions with HYL1^{WT} (*SI Appendix*, Fig. S7 *E–G*).

We further performed an in vitro processing assay using an immunoprecipitated microprocessor complex and radioactive UTP, incorporating pri-miR166 as a substrate (Fig. 3 *M* and *N*). This assay showed that the overexpression of HYL1^{K154A}-6Myc impedes the processing efficiency of pri-miRNAs, although HYL1^{K154A} has almost normal RNA-binding activity and SE and DCL1 interacting ability. In some instances, indestructible proteins tend to aggregate and hinder the function of their native protein forms (57). Thus, we used ultracentrifugation to investigate whether HYL1^{K154A} tends to aggregate and found that HYL1^{K154A} did not form aggregates in the cytoplasm (*SI Appendix*, Fig. S7 *H* and *I*). Previously, two studies reported that phosphorylated HYL1 is not functionally eligible for pri-miRNA processing and is preferentially retained in the nucleus in darkness (37, 58). By performing the subcellular fractionation assay, we found that the HYL1^{K154A} was more retained in the nucleus under dark conditions (*SI Appendix*, Fig. S7*J*). These results implied that the abnormal proteolytic regulation of HYL1 could hinder miRNA biogenesis and plant development.

The Coiled-Coil Domain of COP1 E3 Ligase Recognizes HCS1. COP1 positively correlates to HYL1 stability, but the detailed mechanism of COP1 in maintaining HYL1 remained unknown (36). Therefore, we questioned whether COP1 functions as a chaperone for HYL1 or an inhibitor of HCS1. First, to determine whether COP1 physically associates with HCSs or HYL1, we performed an in vitro pull-down assay using recombinant COP1, HYL1, and HCSs. We found that COP1 directly binds to HYL1, HCS1, and AIR3 (Fig. 4 *A* and *B*). COP1 domains are well-defined in their functionality; RING is for ubiquitination, the coiled-coil (CC) domain is for dimerization, and the WD40 domain is for target protein interactions (59) (Fig. 4*C*). Therefore, using an in vitro pull-down assay, we clarified that the interaction domain of COP1 for HYL1 and HCSs is the CC domain (Fig. 4 *D–F*). To further confirm the protein associations in *Arabidopsis*, we conducted co-IP assays using transgenic plants. By applying an α-Myc antibody, we precipitated HCS1-6Myc and AIR3-6Myc from 10-d-old WT/*35S:HCS1-6Myc* and WT/*35S:AIR3-6Myc* transgenic seedlings, and the presence of COP1 in the precipitates was determined with an α-COP1 antibody. We found that COP1 associates with HCS1 in vivo, but not with AIR3 (Fig. 4 *G* and *H*). Likewise, we tested the association between COP1 and HYL1 using 10-d-old Ler/*XVE:-COP1-6Myc* seedlings grown under conditions of β-estradiol (20 μM) supplementation, but its precipitate did not contain endogenous HYL1 when observed using an α-HYL1 antibody (Fig. 4*I*).

To visualize the interaction between COP1 and HCS1 in vivo, we performed a bimolecular fluorescence complementation (BiFC) assay. Consistent with the co-IP assays, COP1-nVenus was associated with both HCS1-cVenus and emitted clear fluorescence in the cytoplasm. We used HIGLE as a HYL1 interacting endonuclease (60) that showed fluorescence in the nucleus as a positive control (*SI Appendix*, Fig. S8*A*). The possibility of nonspecific fluorescence was discounted by testing negative controls (*SI Appendix*, Fig. S8*B*). These results somewhat contradict those of the in vitro pull-down assay. Therefore, we questioned whether COP1 tends to interact with HCS1. We performed an in vitro titration assay and found that the COP1–HCS1 complex was hardly disrupted by the addition of HYL1, implying that COP1 has a higher affinity to HCS1 (Fig. 4*J*). This result may explain why we could not see the COP1–HYL1 association in the light-grown seedlings using an IP assay (Fig. 4*I*).

A previous study showed that four amino acid substitutions hinder the protein-interactive function of the CC domain (61).

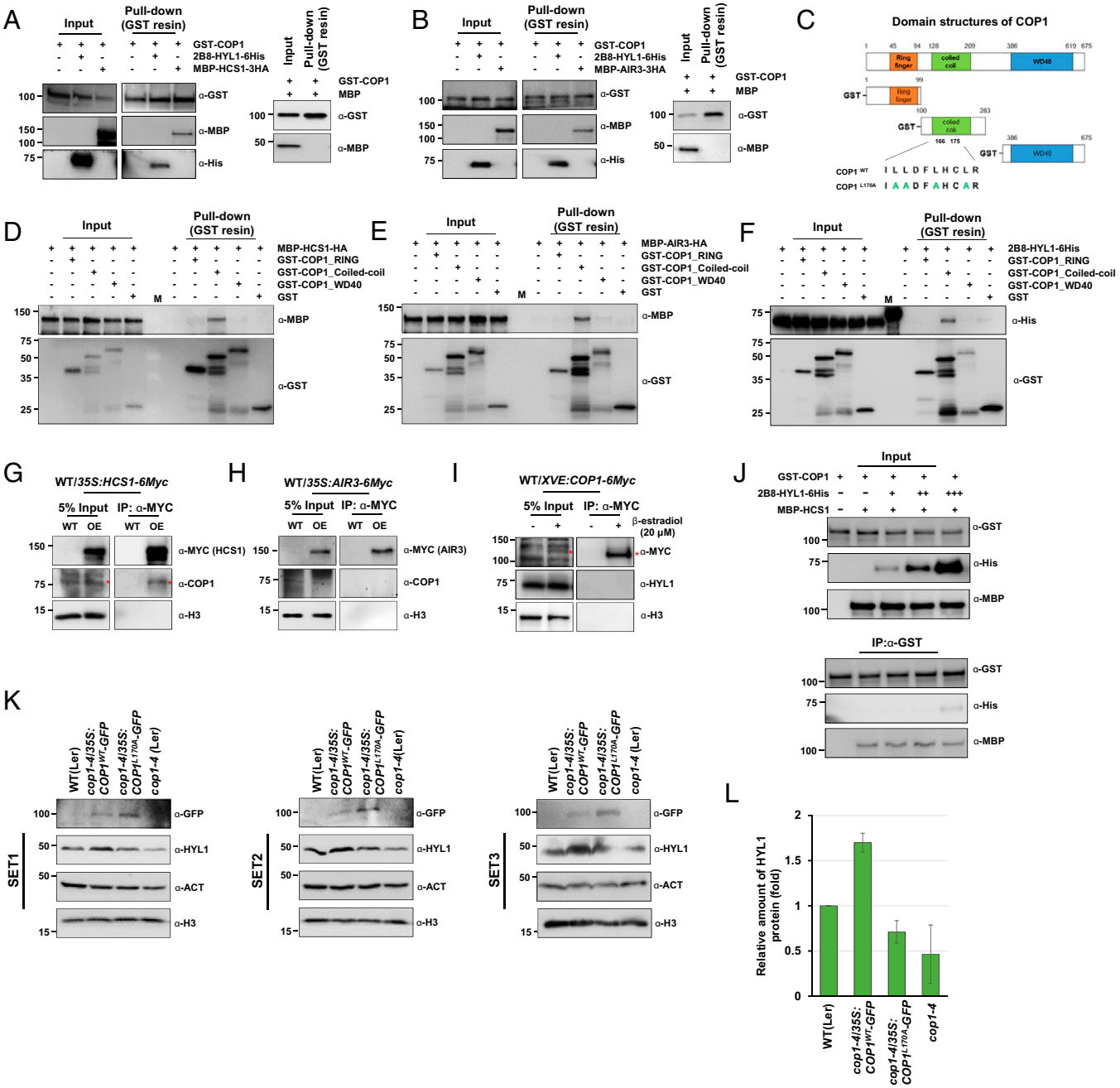

Fig. 4. COP1 directly interacts with HCS1. (*A* and *B*) In vitro pull-down assay of recombinant COP1, HYL1, and HCS1/AIR3. MBP was used as a negative control. (*C*) Schematic of COP1 domain structures. (*D–F*) In vitro pull-down assay of GST-COP1 domains with MBP-HCS1-3HA, MBP-AIR3-3HA, and 2B8-HYL1-6His. GST-COP1 and GST-COP1 domains were used as bait. (*G–I*) Co-IP of HCS1-6Myc, AIR3-6Myc, and COP1-6Myc using 10-d-old plants. Histon3 (H3) was used as a negative control. The red asterisk marks COP1. (*J*) In vitro titration assay of MBP-HCS1-3HA by increasing the concentrations of 2B8-HYL1-6His. (*K* and *L*) The levels of HYL1 in *cop1-4/35S:COP1-GFP* and *cop1-4/35S:COP1^{L170A}-GFP* transgenic plants. Data are the averages of three biological replicates ± SD (n = 3).

Thus, to monitor the role of the CC domain in COP1–HCS1 interaction in vivo, we used *cop1-4/35S:COP1^{L170A}-GFP* transgenic plants expressing the CC mutant (four amino acid substitutions). We found that the reduced HYL1 level in the *cop1-4* mutant was not restored by expressing *35S:COP1^{L170A}-GFP*, while the expression of *35S:COP1-GFP* accumulated ~50% more HYL1 as compared to WT (Fig. 4 *K* and *L*). Collectively, these results indicate that COP1 directly interacts with HCS1, implying that COP1 could be a proteinaceous inhibitor.

CC and WD40 Domains of COP1 Function as the Proteinaceous Inhibitor of HCS1. Next, we tested how COP1 inhibits the proteolytic activity of HCS1 to protect HYL1. To perform the HCS1 inhibition assay, we incubated IP HCS1-6Myc with a fixed amount of recombinant HYL1 (0.2 μg) with or without MBP-COP1. The rapid degradation of HYL1 by HCS1 was blocked by increasing concentrations of MBP-COP1 (0 to 1.5 μg) (Fig. 5 *A* and *B*). We obtained the same results using GST-COP1 as an inhibitor instead of MBP-COP1 (*SI Appendix*, Fig. S9*A*). By applying MBP and GST proteins as negative controls, we confirmed that both MBP

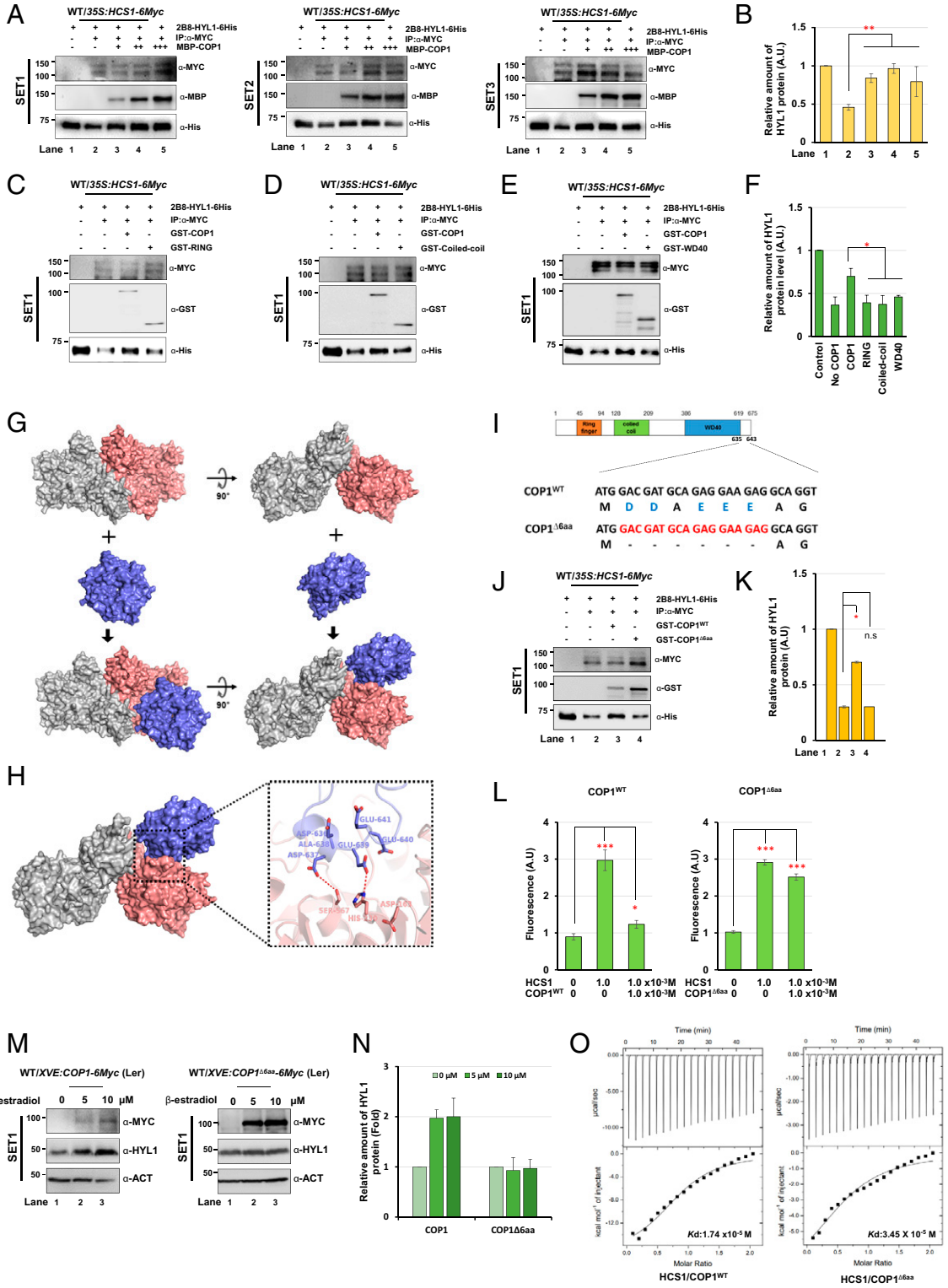

Fig. 5. The CC and WD domains of COP1 are essential in inhibiting HCS1 activity. (*A* and *B*) In vitro HCS1 inhibition assay by the full-length GST-COP1. The asterisk indicates statistical significance, compared between the inhibition assay with and without COP1 (**$P < 0.005$). (*C*–*F*) In vitro HCS1 inhibition assay by GST-COP1 domains. The asterisk indicates statistical significance (*$P < 0.05$). All expression analyses were performed with independent replicates ($n = 3$). (*G*) The complex structure of the HCS1 dimer and the WD40 domain of COP1. Protruding region of WD40 fits into the substrate-binding pocket of HCS1. Monomeric HCS1 and WD40 domain are colored by salmon and slate, respectively. (*H*) Interacting residues of HCS1 and the WD40 domain are shown as a stick model. (*I*) The sequence of negatively charged six amino acids of the COP1-WD40 domain. (*J* and *K*) In vitro HCS1 inhibition assay by GST-COP1 and GST-COP1$^{\Delta 6aa}$. The asterisk indicates statistical significance (*$P < 0.05$). Data are the averages of three replicates ± SD ($n = 3$). (*L*) In vitro HCS1 inhibition assay by GST-COP1, or COP1$^{\Delta 6aa}$, using the IQF peptide substrate. The asterisk indicates statistical significance (*$P < 0.05$, ***$P < 0.0005$). Data are the averages of five replicates ± SD ($n = 5$). (*M* and *N*) Expression level of HYL1 in WT/*XVE:COP1-6Myc* and WT/*XVE:COP1*$^{\Delta 6aa}$*-6Myc* transgenic plants under β-estradiol treatment. Data are the averages of three replicates ± SD ($n = 3$). (*O*) ITC analysis of HCS1 binding affinity with COP1 and COP1$^{\Delta 6aa}$.

and GST fusion tags were irrelevant to the antiprotease activity of COP1 (*SI Appendix*, Fig. S9*B*). Next, we separately applied recombinant RING, CC, and WD40 domain proteins to the in vitro HYL1 degradation assay to define the domain for the proteinaceous inhibitor activity of COP1. Unexpectedly, none of these domains could efficiently block HYL1 degradation in vitro, implying that each domain alone is insufficient for the antiprotease activity of COP1 (Fig. 5 *C–F* and *SI Appendix*, Fig. S9 *C–E*). By performing a low-stringency in vitro pull-down assay, we found that the WD40 domain also interacts with HCS1, even though the CC domain is mainly responsible for the strength of the interaction (*SI Appendix*, Fig. S9*F*). Thus, we speculated that both the CC and WD40 domains might be essential for the inhibitory function of COP1.

Based on the HCS1 and HYL1 binding modes (Fig. 1*P*), we tried to understand the inhibitory action of COP1 on HCS1. Although the whole structure of COP1 was not defined, many RING, CC, WD40 domains (PDB ID code 5IGO) were available on the RCSB Protein Data Bank. WD40 domains, one of the well-defined protein-interacting motifs, exhibit four to eight β-propeller structures that mediate protein–protein interactions with different partners using all sides of its surface (62). Therefore, we could predict three binding modes based on initial docking modeling using the program HEX. In all three binding modes, the WD40 domain seemed to interact with HCS1 through the protruding region (residues 630 to 642) located outside the circularized β-propeller structure, which is highly negatively charged. The first scenario is that the WD40 domain binds to the positively charged region of the subtilase domain of HCS1 (residues 603 to 617) and causes structural transformations. The second is the hindrance of HCS1 dimerization by hijacking the PA domain of HCS1 (residues 411 to 482). Third, the WD40 domain binds to the pocket area of the active site, which can only be formed if the full-length HCS1 is properly folded (*SI Appendix*, Fig. S10 *A–D*). We found that full-length COP1 binds to neither the monomeric PA domain nor the positively charged region of the subtilase domain of HCS1 (*SI Appendix*, Fig. S10 *E* and *F*). Therefore, we selected the third scenario as the most plausible hypothesis: the WD40 domain of COP1 might bind to the active site of HCS1 through its prominent binding region (the C-terminal side of the last β-propeller structure) (Fig. 5 *G* and *H* and *SI Appendix*, Fig. S10*G*).

However, we assumed that the interaction between the active site and the WD40 domain could be maintained by the strong interaction between the CC domain and an unidentified region of HCS1 (Fig. 4*D*). To test whether the WD40 domain is essential for the steric inhibition of HCS1 by COP1, we deleted six amino acids at the protruding region of the WD40 domain ($COP1^{\Delta 6aa}$, deleted 636 to 641) (Fig. 5*I* and *SI Appendix*, Fig. S10*H*). By performing the HCS1 inhibition assay using full-length $COP1^{WT}$ and $COP1^{\Delta 6aa}$, we found that deleting six amino acids notably diminished the inhibitory activity of COP1 (Fig. 5 *J* and *K* and *SI Appendix*, Fig. S10*I*). This result was further confirmed by the HCS1 inhibition assay using IQF peptide substrates (Fig. 5*L*). Next, we confirmed the importance of the WD40 domain in suppressing HCS1 with Ler/*XVE:COP1-6Myc* and Ler/*XVE: COP1*$^{\Delta 6aa}$*-6Myc* transgenic plants (Fig. 5 *M* and *N* and *SI Appendix*, Fig. S10*J*). Indeed, HYL1 levels were unaltered in Ler/*XVE: COP1*$^{\Delta 6aa}$*-6Myc*, while HYL1 levels were elevated in Ler/*XVE:COP1-6Myc* in response to increasing concentration of β-estradiol. Isothermal titration calorimetry (ITC) analysis showed that $COP1^{\Delta 6aa}$ has a binding affinity (K_a) to HCS1 that is twice as low as that of $COP1^{WT}$ (2.9×10^4 M vs. 5.7×10^4 M), which possibly led to the reduction of the proteinaceous inhibitor activity of COP1 (Fig. 5*O*). Taken together, these results suggest that the CC domain may mediate the interaction between COP1 and HCS1, and the WD40 domain could sterically block the active site of HCS1.

Discussion

Subtilases are a highly diverse class of serine proteases found in all three domains of life. During evolution, the functional diversification and complexity of subtilases led to the acquisition of plant-specific functions. In plants, subtilases appear to play key roles in embryogenesis, seed development, germination, cuticle formation, epidermal patterning, vascular development, programmed cell death, organ abscission, senescence, and plant responses to their biotic and abiotic environments (63, 64). Despite the wide range of biological impacts, the molecular functions of most subtilases on their targets remain undefined due to difficulties in target identification. To date, among the 56 subtilases found in *Arabidopsis*, 9 have had their target proteins and molecular and physiological functions reported (65). In addition, we revealed a subtilase that negatively regulates one of the global regulatory pathways, miRNA biogenesis. Given the role of miRNAs in gene expression, HCS1 may be necessary for regulating a variety of biological events.In this study, we revealed several essential features of HCS1-mediated HYL1 degradation. First, HCS1 specifically cleaves the RBD2 domain of HYL1 by recognizing the Arg151-Thr152-Lys153-Lys154 residues. Second, we revealed structural insights into HCS1-mediated HYL1 cleavage by integrating the crystal structure of HYL1 and the homology model of HCS1. Third, we observed redundancy between HCS1 and its paralog AIR3 in the proteolytic regulation of HYL1. Fourth, light/dark transition-induced HYL1 degradation was impeded in *hcs1air3*. Fifth, HYL1-proteostasis seems to be important for miRNA biogenetic regulation; we showed that ectopic expression of the HCS-resistant $HYL1^{K154A}$ mutant hinders miRNA biogenesis, despite its RNA-binding activity and ability for SE and DCL1 interactions. However, it is unclear how $HYL1^{K154A}$ mutant interfered the pri-miRNA processing. Previously, we showed that $HYL1^{NES}$ mutant accumulates more in the nucleus and hinders the HYL1 proteolysis and consequential miRNA biogenesis (37). Thus, we roughly assumed that HYL1-accessiveness could hinder DCL1 for pri-miRNA binding via FHA2, a negative regulator with dual role in strengthening HYL1-RNA but attenuating DCL1-RNA interactions, rather than assisting for precise processing (66). To further clarify this assumption, in vitro reconstitution of DCL1, SE, HYL1, and FHA2 for pri-miRNA processing assay should be performed in a following study.

COP1 is known to shuttle between the cytoplasm and nucleus in response to light/dark transition. The nuclear exclusion of COP1 is thought to contribute to the rapid stabilization of photomorphogenic factors in the nucleus (67, 68). Despite the distinctive localization of COP1, the function of cytoplasmic COP1 previously remained unknown. Our results suggest that cytoplasmic COP1 is a protein inhibitor of HCS1. Protease inhibitors are mainly categorized into catalytic inhibitors and steric blockers (69). For three reasons, we speculate that COP1 may block the active site of HCS1 rather than act as a catalytic inhibitor: first, the K_d value (1.74×10^{-5} M) of the interaction between COP1 and HCS1 is too high for COP1 to be a canonical catalytic inhibitor; second, homology modeling showed that the protruding motif of the WD40 domain fits on the active site of HCS1; and third, the CC domain is essential for the interaction between COP1 and HCS1. Our results provide evidence of the cytoplasmic role of COP1, beyond its well-defined E3 ligase activity and the novel feature of the WD40 domain itself as a docking lid that obstructs substrate access into HCS1. Given that the WD40 domain proteins constitute 1 to 2% of a typical eukaryotic proteome (70), the novel feature of the WD40 domain is worthwhile to discuss in the context of the diverse functions of WD40 domain-containing proteins. Collectively, we propose a regulatory network, the COP1-HYL1-HCS1 pathway, for miRNA biogenesis. Light triggers the nuclear exclusion of COP1, the cytoplasm COP1 inhibits HCS1, and HYL1 enters the nucleus to perform its function. In contrast, light deprivation, or

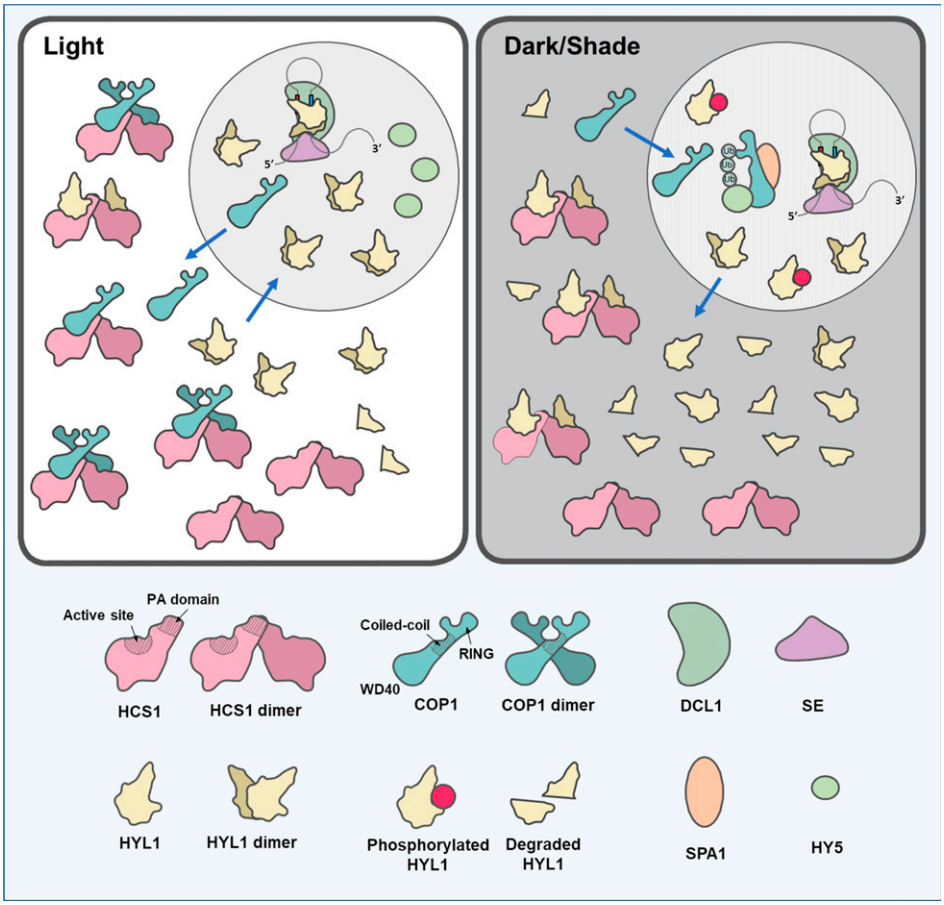

Fig. 6. Graphic of the COP1-HYL1-HCS1 network. Light triggers the cytoplasmic localization of COP1. Cytoplasmic COP1 inhibits HCS1 via direct protein–protein interaction that protects HYL1. Upon light deprivation, COP1 moves back to the nucleus, unshackles HCS1, and degrades light-signaling components, including HY5. Some phosphorylated HYL1 accumulated in the nucleus. Cytoplasmic HYL1 is degraded by HCS1.

shade relocalizes COP1 to the nucleus, and unshackled HCS1 degrades HYL1 (Fig. 6). Taken together, we suggest a regulatory layer in miRNA biogenesis, the subtilase-proteolysis system.

Materials and Methods

All plant materials and growth conditions are described in *SI Appendix*. Additional details of RNA extraction, small RNA-sequencing, EMSA, BiFC, co-IP, pull-down assay, size-exclusion chromatography, LC-MS/MS analysis, microscope analysis, cell fractionation, ITC, FRET, pri-miRNA processing, Western blot, Northern blot, protein cleavage analysis, and protein structural modeling are provided in *SI Appendix*.

Data Availability. All study data are included in the main text and supporting information.

ACKNOWLEDGMENTS. We thank Nam-Chon Paek for providing *cop1-4/35S:COP1^{WT}-GFP* and *cop1-4/35S:COP1^{L170A}-GFP* transgenic plants. This research was supported by the Basic Science Research Program through the National Research Foundation of Korea (NRF), funded by the Ministry of Science, ICT (information and communications technology), and Future Planning (NRF-2020R1A2B5B01002592 and NRF-2018R1A6A1A03025607), and by Samsung Science and Technology Foundation Project SSTF-BA1801-09 (to S.W.Y.). This research was supported in part by NRF-2020R1I1A1A01073842 (to H.J.J.); and Brain Korea 21 (BK21) PLUS program fellowship awards to S.W.C., Y.K.O., M.K.H., C.M., and G.M.K.

1. R. C. Lee, R. L. Feinbaum, V. Ambros, The *C. elegans* heterochronic gene lin-4 encodes small RNAs with antisense complementarity to lin-14. *Cell* **75**, 843–854 (1993).
2. B. Wightman, I. Ha, G. Ruvkun, Posttranscriptional regulation of the heterochronic gene lin-14 by lin-4 mediates temporal pattern formation in *C. elegans*. *Cell* **75**, 855–862 (1993).
3. A. Fire *et al.*, Potent and specific genetic interference by double-stranded RNA in *Caenorhabditis elegans*. *Nature* **391**, 806–811 (1998).
4. P. D. Zamore, T. Tuschl, P. A. Sharp, D. P. Bartel, RNAi: Double-stranded RNA directs the ATP-dependent cleavage of mRNA at 21 to 23 nucleotide intervals. *Cell* **101**, 25–33 (2000).
5. A. J. Hamilton, D. C. Baulcombe, A species of small antisense RNA in posttranscriptional gene silencing in plants. *Science* **286**, 950–952 (1999).
6. D. P. Bartel, MicroRNAs: Genomics, biogenesis, mechanism, and function. *Cell* **116**, 281–297 (2004).
7. Y. Lee, K. Jeon, J.-T. Lee, S. Kim, V. N. Kim, MicroRNA maturation: Stepwise processing and subcellular localization. *EMBO J.* **21**, 4663–4670 (2002).
8. Y. Lee *et al.*, The nuclear RNase III Drosha initiates microRNA processing. *Nature* **425**, 415–419 (2003).
9. T. P. Chendrimada *et al.*, TRBP recruits the Dicer complex to Ago2 for microRNA processing and gene silencing. *Nature* **436**, 740–744 (2005).
10. X. Chen, MicroRNA biogenesis and function in plants. *FEBS Lett.* **579**, 5923–5931 (2005).
11. Y. Kurihara, Y. Watanabe, Arabidopsis micro-RNA biogenesis through Dicer-like 1 protein functions. *Proc. Natl. Acad. Sci. U.S.A.* **101**, 12753–12758 (2004).
12. Y. Kurihara, Y. Takashi, Y. Watanabe, The interaction between DCL1 and HYL1 is important for efficient and precise processing of pri-miRNA in plant microRNA biogenesis. *RNA* **12**, 206–212 (2006).
13. L. Yang, Z. Liu, F. Lu, A. Dong, H. Huang, SERRATE is a novel nuclear regulator in primary microRNA processing in Arabidopsis. *Plant J.*. **47**, 841–850 (2006).
14. N. Baumberger, D. C. Baulcombe, Arabidopsis ARGONAUTE1 is an RNA Slicer that selectively recruits microRNAs and short interfering RNAs. *Proc. Natl. Acad. Sci. U.S.A.* **102**, 11928–11933 (2005).
15. S. M. Hammond, E. Bernstein, D. Beach, G. J. Hannon, An RNA-directed nuclease mediates post-transcriptional gene silencing in Drosophila cells. *Nature* **404**, 293–296 (2000).
16. J. Martinez, A. Patkaniowska, H. Urlaub, R. Lührmann, T. Tuschl, Single-stranded antisense siRNAs guide target RNA cleavage in RNAi. *Cell* **110**, 563–574 (2002).
17. E. Huntzinger, E. Izaurralde, Gene silencing by microRNAs: Contributions of translational repression and mRNA decay. *Nat. Rev. Genet.* **12**, 99–110 (2011).
18. R. Sunkar, Y. F. Li, G. Jagadeeswaran, Functions of microRNAs in plant stress responses. *Trends Plant Sci.* **17**, 196–203 (2012).

19. H. Zhu *et al.*, Arabidopsis Argonaute10 specifically sequesters miR166/165 to regulate shoot apical meristem development. *Cell* **145**, 242–256 (2011).
20. C. Pohl, I. Dikic, Cellular quality control by the ubiquitin-proteasome system and autophagy. *Science* **366**, 818–822 (2019).
21. A. Varshavsky, The ubiquitin system, autophagy, and regulated protein degradation. *Annu. Rev. Biochem.* **86**, 123–128 (2017).
22. D. Gibbings *et al.*, Selective autophagy degrades DICER and AGO2 and regulates miRNA activity. *Nat. Cell Biol.* **14**, 1314–1321 (2012).
23. X. Tang *et al.*, Acetylation of Drosha on the N-terminus inhibits its degradation by ubiquitination. *PLoS One* **8**, e72503 (2013).
24. J. Y. Lee *et al.*, Merlin facilitates ubiquitination and degradation of transactivation-responsive RNA-binding protein. *Oncogene* **25**, 1143–1152 (2006).
25. Q. Han *et al.*, Mechanism and function of antiviral RNA interference in mice. *MBio* **11**, e03278-19 (2020).
26. C. Y. Shi *et al.*, The ZSWIM8 ubiquitin ligase mediates target-directed microRNA degradation. *Science* **370**, eabc9359 (2020).
27. K. Earley, M. Smith, R. Weber, B. Gregory, R. Poethig, An endogenous F-box protein regulates ARGONAUTE1 in *Arabidopsis thaliana*. *Silence* **1**, 15 (2010).
28. N. Baumberger, C.-H. Tsai, M. Lie, E. Havecker, D. C. Baulcombe, The Polerovirus silencing suppressor P0 targets ARGONAUTE proteins for degradation. *Curr. Biol.* **17**, 1609–1614 (2007).
29. D. Bortolamiol, M. Pazhouhandeh, K. Marrocco, P. Genschik, V. Ziegler-Graff, The Polerovirus F box protein P0 targets ARGONAUTE1 to suppress RNA silencing. *Curr. Biol.* **17**, 1615–1621 (2007).
30. T. Csorba, R. Lózsa, G. Hutvágner, J. Burgyán, Polerovirus protein P0 prevents the assembly of small RNA-containing RISC complexes and leads to degradation of ARGONAUTE1. *Plant J.* **62**, 463–472 (2010).
31. B. Derrien *et al.*, Degradation of the antiviral component ARGONAUTE1 by the autophagy pathway. *Proc. Natl. Acad. Sci. U.S.A.* **109**, 15942–15946 (2012).
32. B. Derrien *et al.*, A suppressor screen for AGO1 degradation by the Viral F-Box P0 protein uncovers a role for AGO DUF1785 in sRNA duplex unwinding. *Plant Cell* **30**, 1353–1374 (2018).
33. S. Michaeli *et al.*, The viral F-box protein P0 induces an ER-derived autophagy degradation pathway for the clearance of membrane-bound AGO1. *Proc. Natl. Acad. Sci. U.S.A.* **116**, 22872–22883 (2019).
34. M. H. Chiu, I. H. Chen, D. C. Baulcombe, C. H. Tsai, The silencing suppressor P25 of Potato virus X interacts with Argonaute1 and mediates its degradation through the proteasome pathway. *Mol. Plant Pathol.* **11**, 641–649 (2010).
35. D. A. Ré *et al.*, CURLY LEAF regulates MicroRNA activity by controlling ARGONAUTE 1 Degradation in Plants. *Mol. Plant* **13**, 72–87 (2020).
36. S. K. Cho, S. Ben Chaabane, P. Shah, C. P. Poulsen, S. W. Yang, COP1 E3 ligase protects HYL1 to retain microRNA biogenesis. *Nat. Commun.* **5**, 5867 (2014).
37. N. P. Achkar *et al.*, A Quick HYL1-dependent reactivation of MicroRNA production is required for a proper developmental response after extended periods of light deprivation. *Dev. Cell* **46**, 236–247.e6 (2018).
38. S. W. Choi *et al.*, Light triggers the miRNA-biogenetic inconsistency for de-etiolated seedling survivability in *Arabidopsis thaliana*. *Mol. Plant* **13**, 431–445 (2020).
39. Y. Li *et al.*, Degradation of SERRATE via ubiquitin-independent 20S proteasome to survey RNA metabolism. *Nat. Plants* **6**, 970–982 (2020).
40. D. Basavarajappa *et al.*, Dicer up-regulation by inhibition of specific proteolysis in differentiating monocytic cells. *Proc. Natl. Acad. Sci. U.S.A.* **117**, 8573–8583 (2020).
41. Z. Zhang *et al.*, Valproic acid causes proteasomal degradation of DICER and influences miRNA expression. *PLoS One* **8**, e82895 (2013).
42. L. W. Neuteboom, L. M. Veth-Tello, O. R. Clijdesdale, P. J. Hooykaas, B. J. van der Zaal, A novel subtilisin-like protease gene from *Arabidopsis thaliana* is expressed at sites of lateral root emergence. *DNA Res.* **6**, 13–19 (1999).
43. J. X. Liu, R. Srivastava, S. Howell, Overexpression of an Arabidopsis gene encoding a subtilase (AtSBT5.4) produces a clavata-like phenotype. *Planta* **230**, 687–697 (2009).
44. H. Yamagata, T. Masuzawa, Y. Nagaoka, T. Ohnishi, T. Iwasaki, Cucumisin, a serine protease from melon fruits, shares structural homology with subtilisin and is generated from a large precursor. *J. Biol. Chem.* **269**, 32725–32731 (1994).
45. P. Mahon, A. Bateman, The PA domain: A protease-associated domain. *Protein Sci.* **9**, 1930–1934 (2000).
46. A. Cedzich *et al.*, The protease-associated domain and C-terminal extension are required for zymogen processing, sorting within the secretory pathway, and activity of tomato subtilase 3 (SlSBT3). *J. Biol. Chem.* **284**, 14068–14078 (2009).
47. A. Kurata, K. Uchimura, T. Kobayashi, K. Horikoshi, Collagenolytic subtilisin-like protease from the deep-sea bacterium *Alkalimonas collagenimarina* AC40T. *Appl. Microbiol. Biotechnol.* **86**, 589–598 (2010).
48. K. Murayama *et al.*, Crystal structure of cucumisin, a subtilisin-like endoprotease from *Cucumis melo* L. *J. Mol. Biol.* **423**, 386–396 (2012).
49. A. Tan-Wilson, B. Bandak, M. Prabu-Jeyabalan, The PA domain is crucial for determining optimum substrate length for soybean protease C1: Structure and kinetics correlate with molecular function. *Plant Physiol. Biochem.* **53**, 27–32 (2012).
50. C. Ottmann *et al.*, Structural basis for Ca^{2+}-independence and activation by homodimerization of tomato subtilase 3. *Proc. Natl. Acad. Sci. U.S.A.* **106**, 17223–17228 (2009).
51. R. Rose *et al.*, Purification, crystallization and preliminary X-ray diffraction analysis of a plant subtilase. *Acta Crystallogr. Sect. F Struct. Biol. Cryst. Commun.* **65**, 522–525 (2009).
52. A. Sotokawauchi *et al.*, Structural basis of cucumisin protease activity regulation by its propeptide. *J. Biochem.* **161**, 45–53 (2017).
53. R. Rose, A. Schaller, C. Ottmann, Structural features of plant subtilases. *Plant Signal. Behav.* **5**, 180–183 (2010).
54. S. W. Yang *et al.*, Structure of Arabidopsis HYPONASTIC LEAVES1 and its molecular implications for miRNA processing. *Structure (London, England: 1993)* **18**, 594–605 (2010).
55. D. W. Ritchie, Recent progress and future directions in protein-protein docking. *Curr. Protein Pept. Sci.* **9**, 1–15 (2008).
56. C. Dominguez, R. Boelens, A. M. Bonvin, HADDOCK: A protein-protein docking approach based on biochemical or biophysical information. *J. Am. Chem. Soc.* **125**, 1731–1737 (2003).
57. A. Falsone, S. F. Falsone, Legal but lethal: Functional protein aggregation at the verge of toxicity. *Front. Cell. Neurosci.* **9**, 45 (2015).
58. C. Su *et al.*, The protein phosphatase 4 and SMEK1 complex dephosphorylates HYL1 to promote miRNA biogenesis by antagonizing the MAPK cascade in Arabidopsis. *Dev. Cell* **41**, 527–539.e5 (2017).
59. S. Uljon *et al.*, Structural basis for substrate selectivity of the E3 Ligase COP1. *Structure* **24**, 687–696 (2016).
60. S. K. Cho *et al.*, HIGLE is a bifunctional homing endonuclease that directly interacts with HYL1 and SERRATE in *Arabidopsis thaliana*. *FEBS Lett.* **591**, 1383–1393 (2017).
61. B. D. Lee *et al.*, The F-box protein FKF1 inhibits dimerization of COP1 in the control of photoperiodic flowering. *Nat. Commun.* **8**, 2259 (2017).
62. C. Xu, J. Min, Structure and function of WD40 domain proteins. *Protein Cell* **2**, 202–214 (2011).
63. A. Schaller *et al.*, From structure to function—A family portrait of plant subtilases. *New Phytol.* **218**, 901–915 (2018).
64. J. Figueiredo, M. Sousa Silva, A. Figueiredo, Subtilisin-like proteases in plant defence: The past, the present and beyond. *Mol. Plant Pathol.* **19**, 1017–1028 (2018).
65. C. Rautengarten *et al.*, Inferring hypotheses on functional relationships of genes: Analysis of the *Arabidopsis thaliana* subtilase gene family. *PLOS Comput. Biol.* **1**, e40 (2005).
66. S. J. Park *et al.*, Light-stabilized FHA2 suppresses miRNA biogenesis through interactions with DCL1 and HYL1. *Molecular Plant* **14**, 647–663 (2021).
67. A. G. von Arnim, X. W. Deng, Light inactivation of Arabidopsis photomorphogenic repressor COP1 involves a cell-specific regulation of its nucleocytoplasmic partitioning. *Cell* **79**, 1035–1045 (1994).
68. M. Pacín, M. Legris, J. J. Casal, Rapid decline in nuclear costitutive photomorphogenesis1 abundance anticipates the stabilization of its target elongated hypocotyl5 in the light. *Plant Physiol.* **164**, 1134–1138 (2014).
69. J. Otlewski, F. Jelen, M. Zakrzewska, A. Oleksy, The many faces of protease-protein inhibitor interaction. *EMBO J.* **24**, 1303–1310 (2005).
70. Q. Li *et al.*, Genome-wide analysis of the WD-repeat protein family in cucumber and Arabidopsis. *Mol. Genet. Genomics* **289**, 103–124 (2014).